SIAM J. NUMER. ANAL.
Vol. 55, No. 4, pp. 1867–1891

A PARTIAL FOURIER TRANSFORM METHOD FOR A CLASS OF HYPOELLIPTIC KOLMOGOROV EQUATIONS*

CHRISTOPH REISINGER†, ENDRE SÜLI†, AND ALAN WHITLEY†

Abstract. We consider hypoelliptic Kolmogorov equations in $n+1$ spatial dimensions with $n \geq 1$, where the differential operator in the first n spatial variables featuring in the equation is second-order elliptic, and with respect to the $(n+1)$st spatial variable the equation contains a pure transport term only and is therefore first-order hyperbolic. If the two differential operators, in the first n and in the $(n+1)$st co-ordinate directions, do not commute, we benefit from hypoelliptic regularization in time, and the solution for $t > 0$ is smooth even for a Dirac initial datum prescribed at $t = 0$. We study specifically the case where the coefficients depend only on the first n variables. In that case, a Fourier transform in the last variable and standard central finite difference approximation in the other variables can be applied for the numerical solution. We prove second-order convergence in the spatial grid size for the model hypoelliptic equation $\frac{\partial u}{\partial t} + x\frac{\partial u}{\partial y} = \frac{\partial^2 u}{\partial x^2}$ subject to the initial condition $u(x, y, 0) = \delta(x) \otimes \delta(y)$ with $(x, y) \in \mathbb{R} \times \mathbb{R}$ and $t > 0$, proposed by Kolmogorov, and we also consider an extension of this problem with $n = 2$. We demonstrate exponential convergence of an approximation of the inverse Fourier transform based on the trapezium rule.

Key words. hypoelliptic equations, Kolmogorov equation, Dirac initial datum, Fourier methods, finite difference methods

AMS subject classifications. 65N06, 35H10, 35Q84, 65T50

DOI. 10.1137/16M1076654

1. Introduction.

This paper is concerned with the numerical solution of initial-value problems for a class of partial differential equations, subject to Dirac initial datum, which have the form

$$\frac{\partial u}{\partial t} + c(x,t)\frac{\partial u}{\partial y} = \mathcal{L}u, \qquad (x, y, t) \in \mathbb{R}^n \times \mathbb{R} \times (0, T], \tag{1.1}$$

$$u(x, y, 0) = \delta(x - x_0) \otimes \delta(y - y_0), \qquad (x, y) \in \mathbb{R}^n \times \mathbb{R}, \tag{1.2}$$

where $n \geq 1$, $T > 0$, $x_0 \in \mathbb{R}^n$, $y_0 \in \mathbb{R}$, the symbol $\otimes$ signifies the (associative) binary operation of tensor product of distributions, the drift coefficient $c = c(x, t)$ is independent of the variable $y \in \mathbb{R}$, $\nabla_x c(x, t) \neq 0$ for all $(x, t) \in \mathbb{R}^n \times (0, T]$, and the elliptic differential operator $\mathcal{L}$ does not include any y-derivatives and its coefficients only depend on $x = (x_1, \ldots, x_n) \in \mathbb{R}^n$ and $t \in [0, T]$; in other words, $\mathcal{L}$ is assumed to be of the form

$$\mathcal{L} = \sum_{i,j=1}^{n} a_{ij}(x,t)\frac{\partial^2}{\partial x_i \partial x_j} + \sum_{i=1}^{n} b_i(x,t)\frac{\partial}{\partial x_i} + d(x,t), \tag{1.3}$$

where a_{ij}, $i, j = 1, \ldots, n$, b_i, $i = 1, \ldots n$, and d are continuous functions of $(x, t) \in \mathbb{R}^n \times [0, T]$, and there exists a constant $c_0 > 0$ such that

$$\sum_{i,j=1}^{n} a_{ij}(x,t)\,\xi_i\xi_j \geq c_0|\xi|^2 \qquad \forall\, \xi = (\xi_1, \ldots, \xi_n) \in \mathbb{R}^n \quad \forall\, (x,t) \in \mathbb{R}^n \times [0,T].$$

*Received by the editors May 23, 2016; accepted for publication (in revised form) May 10, 2017; published electronically July 26, 2017.

http://www.siam.org/journals/sinum/55-4/M107665.html

†Mathematical Institute, University of Oxford, Andrew Wiles Building, Oxford OX2, UK (reisinge@maths.ox.ac.uk, https://people.maths.ox.ac.uk/reisinge/, suli@maths.ox.ac.uk, https://people.maths.ox.ac.uk/suli/, whitley@maths.ox.ac.uk).

Hypoelliptic problems of this kind arise naturally from statistical physics, stochastic analysis, and mathematical finance in particular, as Kolmogorov equations that describe the evolution of the probability density function of stochastic processes; the initial datum in such problems is frequently a point source, which is modelled by a Dirac measure concentrated at a point. Such initial conditions are clearly also relevant in the construction of Green's functions. For the definition of hypoellipticity and necessary and sufficient conditions for C^∞ regularity see [7]. Contemporary applications and extensions to nonlinear problems are found in [18], [19].

Given the interest in this class of equations, methods have recently been put forward for their numerical approximation, with a focus on preserving the long-time behavior of solutions to the original equation. In [4], a self-similar change of variables was performed and convergence of the numerical solution to the steady state under these new variables was established; furthermore, an operator splitting scheme based on decomposing the hypoelliptic operator into coercive and convective terms was proposed. In contrast, in [12] asymptotic properties of standard central finite difference schemes were analyzed and decay rates of difference quotients were proved in the case of L^2 initial data. The analysis in those papers does not cover the case of Dirac initial data, which are important in a number of applications, and indeed the numerical experiments at the end of this section show that in the case of Dirac initial datum convergence of a finite difference approximation to the problem based on central differences is not guaranteed in either the discrete L^2 or maximum norm.

The semidiscrete Fourier scheme that we propose here for the numerical approximation of problem (1.1) involves the application of a Fourier transform to (1.1) in the y-direction (y-FT) to reduce the dimension of the problem by transforming it into a one-parameter family of parabolic problems, and it then applies finite difference discretization in the x-direction to this parametrized family of parabolic problems, followed by the application of an inverse Fourier transform. The observed exponential convergence of the numerical approximation to the inverse Fourier transform reduces the computational complexity of the proposed scheme to that of a finite difference approximation of a problem that has no dependence on y, as long as the solution is required for a single value of y only. The application of the y-FT avoids the use of lower-order stable upwind or semi-Lagrangian discretizations of the y-derivative; for alternative, higher-order semi-Lagrangian discretizations, see, for example, [1], [16], [2], and the references therein. Moreover, it transforms the Dirac initial datum into a constant function in the y-direction, which is easier to handle numerically. To the best of our knowledge, the numerical scheme proposed in this paper is the first numerical method for hypoelliptic problems of this type which is proved to be convergent for Dirac initial datum.

We shall study in-depth the stylized problem

$$\frac{\partial u}{\partial t} + x\frac{\partial u}{\partial y} = \frac{\partial^2 u}{\partial x^2}, \qquad (x, y, t) \in \mathbb{R} \times \mathbb{R} \times (0, T], \tag{1.4}$$

$$u(x, y, 0) = \delta(x) \otimes \delta(y), \qquad (x, y) \in \mathbb{R} \times \mathbb{R}. \tag{1.5}$$

This is the partial differential equation originally considered by Kolmogorov in his 1934 paper [9]. The significance of this simple toy model stems from the fact that it incorporates two important features: hypoellipticity and Dirac initial datum. Equation (1.4) results from (1.3) for $d \equiv 0$ by shifting the point (x_0, y_0) at which the initial Dirac datum is concentrated to the origin, linearization of the coefficient c with respect to the y variable around $y = 0$, translation in the y-direction with $c(0, 0)t$,

and finally freezing the coefficients c, b, and a with respect to t. Since the final term in (1.3) does not affect the ideas presented herein, for the sake of simplicity of the exposition we shall confine ourselves to the case of $d \equiv 0$. Subject to sign change, our model equation (1.4) coincides with the one studied in [12].

Because of the special structure of the equation (1.4), we shall apply Fourier methods in the construction of its numerical approximation and also in the convergence analysis of the proposed numerical algorithms. We shall explore the behavior of two numerical schemes for the solution of our toy model: a semidiscrete Fourier method and a fully discrete Fourier method, which will be described below.

Whereas the proposed numerical techniques apply to the more general model problem (1.1), (1.2), and, in fact, with more general probability measures as initial data than the Dirac measure considered herein, for the sake of simplicity and clarity of the exposition the mathematical analysis of the proposed numerical method is restricted to the simplified model (1.4), (1.5), which is a special case of the Cauchy problem (1.1), (1.2) above. For this toy model, we shall prove the convergence of the semidiscrete Fourier method and derive expressions for the leading-order terms in the global discretization error. In particular, we shall analyze the behavior of the error between the analytical solution and its numerical approximation and will establish the rate of convergence of the scheme as the spatial discretization parameter $\Delta x \to 0$. It should be noted that this analysis only relates to the analytical solution of the semidiscrete scheme (2.5) and its subsequent exact y-FT inversion. We shall discuss the additional approximations involved in discretizations of these in section 5.

We approach the task of error analysis by applying the inverse Fourier transform to the error between W and w, where W is the solution of the equation resulting from Fourier transforming (1.4) with respect to y, discretizing with respect to x, and applying a discrete Fourier transform with respect to x, whereas w is the solution of the equation resulting from Fourier transforming (1.4) with respect to both x and y. We then perform a wavenumber analysis of the resulting expressions to establish convergence. This method is based on similar ideas to those in [3] and [14], where time stepping schemes for the one-dimensional heat equation with Dirac initial datum were analyzed. While in the cited papers the Fourier transform was used purely as a mathematical tool in the analysis of the discretization error in the original space-time coordinates, here we use a partial Fourier transform (i.e., we transform in the y-variable only) in the construction of the actual numerical method and use a double-Fourier transform (i.e., the Fourier transform in both the x and the y variable) to quantify the error of this approximation. An interesting feature of the present analysis is the intricate interplay between the x- and y-Fourier modes, due to the hypoellipticity of the equation.

In order to motivate the numerical method proposed in the next section, we illustrate the smoothing and convergence properties of the central difference scheme with implicit Euler time stepping, i.e., we consider the finite difference scheme

$$\frac{U_{j,k}^{n+1} - U_{j,k}^{n}}{\Delta t} + x_j \frac{U_{j,k+1}^{n+1} - U_{j,k-1}^{n+1}}{2\Delta y} = \frac{U_{j+1,k}^{n+1} - 2U_{j,k}^{n+1} + U_{j-1,k}^{n+1}}{\Delta x^2}$$

with $(j,k) \in \mathbb{Z}^2$ and $n \geq 0$. This is the scheme studied in [12]; it is shown there in particular that, for $\ell^2(\mathbb{Z}^2)$ initial data, the $\ell^2(\mathbb{Z}^2)$ norms of the first-order difference quotients in the x- and y-directions decay as t^{-1} and t^{-3}, respectively, as $t \to \infty$. Closer to the situation in the present paper, let us consider, instead, a Dirac delta concentrated at the origin in the (x,y)-plane. We approximate the Dirac initial datum

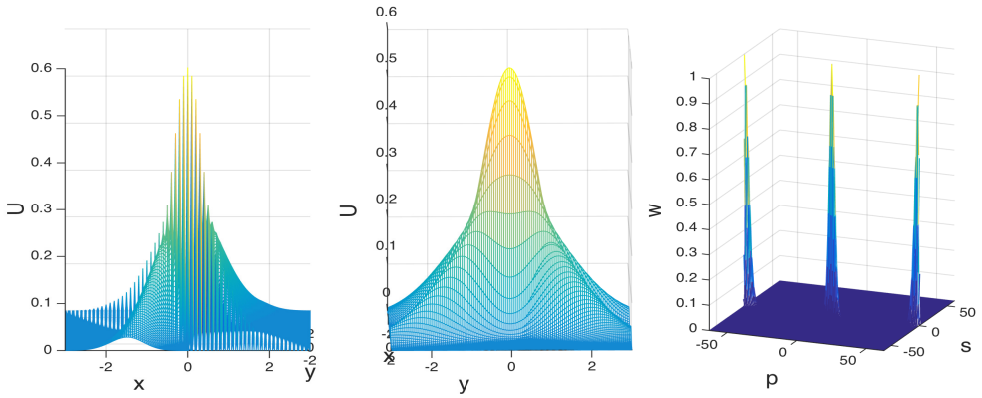

FIG. 1. *Central difference scheme with Dirac initial datum; the computational domain is* $x \in [-10, 10]$, $y \in [-10, 10]$ *(with a smaller plot range); the numerical solution at* $T = 1$ *with* $n_x = n_y = n_t = 400$ *grid spacings in the* x*-,* y*-, and* t*-direction, respectively; left and center the numerical solution viewed along the* y*- and* x*-axes, respectively; right its discrete Fourier transform, with* s *and* p *signifying wavenumbers corresponding to the* x *and* y *co-ordinate directions, respectively.*

by

$$U^0_{j,k} = \begin{cases} \frac{1}{\Delta x\,\Delta y} & \text{for } (j,k) = (0,0), \\ 0 & \text{for } (j,k) \neq (0,0), \end{cases} \qquad (j,k) \in \mathbb{Z}^2,$$

which can be viewed as the mollification of the Dirac measure concentrated at the origin through convolution, in the sense of distributions, with the scaled characteristic function $\frac{1}{\Delta x\,\Delta y}\chi_{[-\Delta x/2,\Delta x/2]\times[-\Delta y/2,\Delta y/2]}$ with unit $L^1(\mathbb{R}^2)$ norm (cf. [8]). We shall consider the problem on a sufficiently large square domain $(-L, L) \times (-L, L)$ in the (x, y)-plane with zero Dirichlet boundary condition at the domain boundary; in our numerical experiment below we took $L = 10$, which ensures that the Dirichlet boundary condition has negligible influence on the values of the numerical solution at the final time of interest, $T = 1$ in our case.

Figure 1, left and center, shows the numerical solution at $T = 1$ from different angles, exhibiting rapid oscillations in the x-direction, but smoothness in the y-direction. Indeed, good approximation to the analytical solution is visible between the oscillations. The discrete Fourier transform of the numerical solution, with wavenumbers s and p (described in more detail later), is depicted in the right panel in Figure 1. It shows low wavenumber components in both s and p near the origin in Fourier space, which approximate well the Fourier transform of the analytical solution, and low s-/high p-wavenumber components concentrated at $(s, p) = (0, \pm\pi/\Delta y) = (0, \pm 20\pi) \approx (0, \pm 63)$, which trigger the spurious oscillations in the numerical approximation of the analytical solution.

Extending the techniques from [3], the time-discrete evolution of the discrete Fourier transform W of the numerical solution U is found to be governed by the recursion (see also sections 3.1 and especially 5.5)

$$\left(1 + 4\frac{\Delta t}{\Delta x^2}\sin^2\left(\frac{s\Delta x}{2}\right)\right) W^{n+1}(s,p) = W^n(s,p) + \frac{\Delta t}{\Delta y}\sin(p\Delta y)\frac{\partial W^{n+1}}{\partial s}(s,p), \; n \geq 0,$$
$$W^0(s,p) = 1$$

for all $(s,p) \in [-\frac{\pi}{\Delta x}, \frac{\pi}{\Delta x}] \times [-\frac{\pi}{\Delta y}, \frac{\pi}{\Delta y}]$. Setting $s = 0$ and $p = \pm\pi/\Delta y$ we deduce that

$$W^n(0, \pm\pi/\Delta y) = 1 \qquad \forall\, n \geq 1.$$

This finding is in line with our numerical tests suggesting that the numerical solution will not converge to the analytical solution as $\Delta x, \Delta y \to 0$ in either $\ell^2(\mathbb{Z}^2)$ or $\ell^\infty(\mathbb{Z}^2)$.

Replacing the central y-difference with an upwind y-difference is observed to produce a convergent sequence of numerical approximations to the analytical solution in the case of a Dirac initial datum, just as for smooth initial data, but such a finite difference scheme is only of first-order accuracy with respect to Δy. We shall therefore propose in the next section a numerical scheme applied to the analytical y-Fourier transform which does not suffer from this shortcoming.

The remainder of the article is structured as follows. In section 2 we introduce the semidiscrete Fourier scheme and formulate the discretization of the toy model (1.4), (1.5); in section 3 we prove that the scheme is second-order convergent in Δx in the space-time ℓ^∞ norm. In section 4, we give an extension of the convergence analysis of the scheme to the case of $n = 2$, i.e., when the diffusion operator acts in two spatial directions, $x = (x_1, x_2)$, while in the third spatial direction, y, there is only a transport term present in the equation; in other words, there is no diffusion in the y-direction. Next, in section 5, we describe aspects of the numerical implementation including the exponential convergence in Δp, the grid size of the Fourier variable in the y-direction, and present numerical results for the toy model (1.4), (1.5). Our findings are summarized in the concluding section.

2. The semidiscrete Fourier scheme. We consider the Fourier transform in the y-direction (briefly, y-FT), defined by

$$v(x,p,t) := \int_{-\infty}^{\infty} u(x,y,t)\, \mathrm{e}^{ipy}\, \mathrm{d}y, \qquad x \in \mathbb{R},\ p \in \mathbb{R},\ t > 0,$$

where it is tacitly understood that the function $y \in \mathbb{R} \mapsto u(x,y,t) \in \mathbb{R}$ is an element of $L^1(\mathbb{R})$ for all $(x,t) \in \mathbb{R}^n \times (0,\infty)$. The Fourier transform in the y-direction of the initial Dirac measure $\delta(x - x_0) \otimes \delta(y - y_0)$ at $t = 0$ is to be understood in the sense of distributions and is equal to $\delta(x - x_0) \otimes \mathrm{e}^{ipy_0}$.

Application of the Fourier transform to (1.1) yields

$$\frac{\partial v}{\partial t} - ipc(x,t)v = \mathcal{L}v, \qquad x \in \mathbb{R},\ p \in \mathbb{R},\ t > 0,$$

which is a family of PDEs in x and t, parametrized by p, for the y-FT: $v(x,p,t)$. We then discretize the operator $\mathcal{L}$ from (1.3) in the x-direction(s) by means of a standard finite difference scheme, using equally spaced grid points, with spacing Δx, but we keep the time variable continuous for the moment at least. This leads to a system of ordinary differential equations (ODEs) indexed by the x-grid points, x_j, and also by the Fourier wavenumber in the y-direction, which we are denoting by p, for the function $V_j(p,t)$. After solving this system of ODEs (in practice numerically, for a finite set of grid points x_j subject to an artificial/numerical Dirichlet boundary condition at the "far-field," and a finite set of y-wavenumbers, $\{p_l\}_{l=l_{\min}}^{l_{\max}}$), we use the inverse y-FT to compute an approximate solution, $U(x_j,y,t)$, in the original coordinates as

$$U(x_j,y,t) = \frac{1}{2\pi} \int_{-2t/(\Delta x)^r}^{2t/(\Delta x)^r} V_j(p,t)\, \mathrm{e}^{-iyp}\, \mathrm{d}p. \tag{2.1}$$

The truncation of the p-integration range in the inversion (2.1) from $p \in (-\infty, \infty)$ to the truncated range $p \in (-2t/(\Delta x)^r, 2t/(\Delta x)^r)$, for a suitable $r > 0$, is dictated by the practical requirement to carry out numerical integration over a finite range. The scaling with $2t$ simplifies the numerical analysis, but of course in practice any suitable scaling would be chosen empirically.

To find the approximation $U_{j,k}(t)$ to $u(x_j, y_k, t)$ numerically, we apply a uniformly spaced and equally weighted quadrature rule to (2.1) and obtain

$$U_{j,k}(t) := \frac{\Delta p}{2\pi} \sum_{l=l_{\min}}^{l_{\max}} V_j(p_l, t)\, \mathrm{e}^{-iy_k p_l} \tag{2.2}$$

for a given k, $l_{\max} > 0$, $l_{\min} < 0$, $l_{\max}\Delta p = -l_{\min}\Delta p = 2t\Delta x^{-r}$. We will also denote $n_p := l_{\max} - l_{\min} + 1$. The numerical results will be seen to exhibit exponential convergence of the p-quadrature (see below and [17]). For an efficient implementation of (2.2), if the solution is needed for several values of k, the fast Fourier transform (FFT) can be used.

We illustrate the method by applying it to the Cauchy problem (1.4) and (1.5), with the aim to analyze the stability and accuracy of the numerical scheme we develop below.

By applying the y-FT to (1.4) and (1.5) we get

$$\frac{\partial v}{\partial t} - ipxv = \frac{\partial^2 v}{\partial x^2}, \qquad (x, p, t) \in \mathbb{R} \times \mathbb{R} \times (0, T], \tag{2.3}$$

$$u(x, p, 0) = \delta(x), \qquad (x, p) \in \mathbb{R} \times \mathbb{R}, \tag{2.4}$$

and we then discretize this one-parameter family of Cauchy problems in the x-direction only, using central differencing with spacing $\Delta x > 0$, to obtain, for $x_j = j\Delta x$, $j \in \mathbb{Z}$,

$$\frac{\partial V_j(p,t)}{\partial t} - ipx_j V_j(p,t) = \frac{V_{j+1}(p,t) - 2V_j(p,t) + V_{j-1}(p,t)}{\Delta x^2},\ p \in \mathbb{R},\ t \in (0, T], \tag{2.5}$$

so that the function $V_j(p,t)$, which approximates $v(x_j, p, t)$, satisfies this equation for each $j \in \mathbb{Z}$ and for all $(p,t) \in \mathbb{R} \times (0,T]$. The initial condition we use for this parametrized ODE system is

$$V_j(p,0) = \begin{cases} 0 & \text{for } j \neq 0, \\ \frac{1}{\Delta x} & \text{for } j = 0 \end{cases} \tag{2.6}$$

for all $p \in \mathbb{R}$, which approximates (2.4).

Remark 1. Alternative approximations to the initial datum are possible instead of (2.6), which results from convolving the Dirac function in the x-direction with an indicator function with support $[-\Delta x/2, \Delta x/2]$. One possibility is to replace the indicator function by a linear spline centered at 0 and with support $[-k\Delta x, k\Delta x]$ for some $k \in \mathbb{Z}_+$, normalized to integrate to 1. The case $k = 1$ leads again to (2.6). The Fourier analysis and numerical tests for the one-dimensional heat equation in [14] show that the choice $k = 2$ can lead to slightly smaller discretization error than $k = 1$, while for larger k the error increases. As we are only concerned with second-order

finite differences in the x-direction, using approximations based on convolution with higher-order B-splines (cf. [8, sections 1.9.2–1.9.4]) will not lead to improvements of the order of convergence.

3. Analysis of the numerical method for the stylized problem. In this section, we will prove the following theorem, which is one of our main results.

THEOREM 3.1. *Let u be the solution to the Cauchy problem* (1.4), (1.5), *and let U be given by* (2.1), (2.5), (2.6). *Then, for any $r > 0$ in* (2.1), *we have that*

$$U(x_j, y, t) - u(x_j, y, t) \;=\; C(x_j, y, t)\,\Delta x^2 + o(\Delta x^2), \qquad j \in \mathbb{Z},\ y \in \mathbb{R},\ t > 0,$$

where

$$C(x_j, y, t) := \left[\frac{t}{2\pi^2}\left(\frac{1}{4!}\left(\frac{\partial}{\partial x} + \frac{t}{2}\frac{\partial}{\partial y}\right)^4 + \frac{1}{5!}\left(\frac{t}{2}\frac{\partial}{\partial y}\right)^4\right) u\right]\Bigg|_{(x_j, y, t)}. \tag{3.1}$$

3.1. The time evolution of the numerical double transform. To investigate the stability and accuracy of the numerical scheme, we use techniques motivated by those in [3] and [14]. Thus, given a set of values $\{f_j\}_{j\in\mathbb{Z}} \in \ell^1(\mathbb{Z})$, on a uniformly-spaced grid $\{x_j\}_{j\in\mathbb{Z}}$ of spacing $\Delta x > 0$ on $\mathbb{R}$, we consider the (semi)discrete Fourier transform

$$\widehat{f}(s) := \Delta x \sum_{j=-\infty}^{\infty} f_j\, \mathrm{e}^{isx_j}, \qquad s \in \left[-\frac{\pi}{\Delta x}, \frac{\pi}{\Delta x}\right],$$

and the inverse of this transform,

$$f_j = \frac{1}{2\pi}\int_{-\frac{\pi}{\Delta x}}^{\frac{\pi}{\Delta x}} \widehat{f}(s)\, \mathrm{e}^{isx_j}\, \mathrm{d}s, \qquad j \in \mathbb{Z}$$

(see, e.g., [10]). We note that the method of analysis here is specific to (1.4) and its higher-dimensional variants (see the extended version of this paper [13]), but the numerical algorithm itself is not, as we demonstrate through the numerical example considered in [13, section 5].

Then, by applying the semidiscrete x-FT to the system of ODEs (2.5), we find

$$\begin{aligned}
&\frac{\partial W(s,p,t)}{\partial t} - p\frac{\partial W(s,p,t)}{\partial s} \\
&\quad= \sum_{j=-\infty}^{\infty} \frac{\partial V_j(p,t)}{\partial t}\, \mathrm{e}^{isx_j}\Delta x - ip \sum_{j=-\infty}^{\infty} x_j V_j(p,t)\, \mathrm{e}^{isx_j}\Delta x \\
&\quad= \sum_{j=-\infty}^{\infty} \frac{V_{j+1}(p,t)\, \mathrm{e}^{isx_j} - 2V_j(p,t)\, \mathrm{e}^{isx_j} + V_{j-1}(p,t)\, \mathrm{e}^{isx_j}}{\Delta x^2}\,\Delta x \\
&\quad= W(s,p,t)\,\frac{4}{\Delta x^2}\sin^2\left(\frac{s\Delta x}{2}\right), \qquad (s,p) \in \left[-\frac{\pi}{\Delta x}, \frac{\pi}{\Delta x}\right] \times \mathbb{R},\ t > 0.
\end{aligned}$$

As $W(s,p,0) = 1$, it follows by the method of characteristics that $W(s,p,t) > 0$ for all $t > 0$, and therefore

$$\frac{\partial \log W}{\partial t} - p\frac{\partial \log W}{\partial s} = \frac{4}{\Delta x^2}\sin^2\left(\frac{s\Delta x}{2}\right), \qquad (s,p) \in \left[-\frac{\pi}{\Delta x}, \frac{\pi}{\Delta x}\right] \times \mathbb{R},\ t > 0.$$

In contrast, taking the x-FT of (2.3), the true double Fourier transform satisfies

$$\frac{\partial w}{\partial t} - p\frac{\partial w}{\partial s} = -s^2 w, \qquad (s,p) \in \mathbb{R}^2,\ t > 0.$$

Since $w(s,p,0) = 1$, and therefore, by the method of characteristics $w(s,p,t) > 0$ for all $t > 0$, we have that

$$\frac{\partial \log w}{\partial t} - p\frac{\partial \log w}{\partial s} = -s^2, \qquad (s,p) \in \mathbb{R}^2,\ t > 0. \tag{3.2}$$

Then, by defining

$$Z(s,p,t) = \log\left(\frac{W(s,p,t)}{w(s,p,t)}\right), \qquad (s,p) \in \left[-\frac{\pi}{\Delta x}, \frac{\pi}{\Delta x}\right] \times \mathbb{R},\ t \geq 0,$$

we find that

$$\frac{\partial Z(s,p,t)}{\partial t} - p\frac{\partial Z(s,p,t)}{\partial s} = s^2 - \frac{4}{\Delta x^2}\sin^2\left(\frac{s\Delta x}{2}\right), \quad (s,p) \in \left[-\frac{\pi}{\Delta x}, \frac{\pi}{\Delta x}\right] \times \mathbb{R},\ t > 0,$$

where

$$g(s) = s^2 - \frac{4}{\Delta x^2}\sin^2\left(\frac{s\Delta x}{2}\right), \qquad s \in \left[-\frac{\pi}{\Delta x}, \frac{\pi}{\Delta x}\right],$$

and $Z(s,p,0) = 0$. We can solve for $Z(s,p,t)$ to obtain

$$Z(s,p,t) = \frac{1}{p}\int_s^{s+pt} g(\sigma)\,\mathrm{d}\sigma, \qquad (s,p) \in \left[-\frac{\pi}{\Delta x}, \frac{\pi}{\Delta x}\right] \times \mathbb{R},\ t \geq 0.$$

Finally, we have

$$W(s,p,t) = w(s,p,t)\exp\left(\frac{1}{p}\int_s^{s+pt} g(\sigma)\,\mathrm{d}\sigma\right), \qquad (s,p) \in \left[-\frac{\pi}{\Delta x}, \frac{\pi}{\Delta x}\right] \times \mathbb{R},\ t \geq 0, \tag{3.3}$$

an expression for the numerical double transform, W, in terms of the true double transform, w, with the exponential factor on the right-hand side of (3.3) reflecting the error introduced by the finite difference approximation in the x-direction. In fact, one can solve (3.2) with initial datum $w(s,p,0) = 1$ to obtain

$$w(s,p,t) = \exp\left(-s^2 t - spt^2 - \frac{1}{3}p^2 t^3\right), \qquad (s,p) \in \mathbb{R}^2,\ t \geq 0. \tag{3.4}$$

A key observation is that it is more convenient to restate the solution in terms of the variables

$$\eta \ = \ s + \frac{pt}{2}, \qquad \xi \ = \ \frac{pt}{2},$$

in Fourier space, a manifestation of the mixing of Fourier modes due to the lack of commutativity of the differential operators in x and y in (1.4). We will refer to these variables in Fourier space as wavenumbers, and it is only in these new variables that

suitable wavenumber regimes can be defined. Indeed, in these new variables, we get

$$\begin{aligned} W(s,p,t) &= w(s,p,t)\exp\left(\frac{1}{p}\int_s^{s+pt}\sigma^2\,\mathrm{d}\sigma\right)\exp\left(-\frac{1}{p}\int_s^{s+pt}\frac{4}{\Delta x^2}\sin^2\left(\frac{\sigma\Delta x}{2}\right)\mathrm{d}\sigma\right)\\ &= w(s,p,t)\,w(s,p,t)^{-1}\exp\left(-\frac{2}{p\Delta x^2}\int_s^{s+pt}(1-\cos(\sigma\Delta x))\,\mathrm{d}\sigma\right)\\ &= \exp\left(-\frac{2t}{\Delta x^2}(1-\operatorname{sinc}(\xi\Delta x)\cos(\eta\Delta x))\right) \end{aligned} \tag{3.5}$$

for $(s,p)\in[-\frac{\pi}{\Delta x},\frac{\pi}{\Delta x}]\times\mathbb{R}$ and $t\geq 0$, where sinc is the unnormalized sinc function, defined as follows (see, for example, [11]):

$$\operatorname{sinc} x := \frac{\sin x}{x} \qquad \text{for } x\in\mathbb{R}\setminus\{0\} \text{ and } \operatorname{sinc} 0 := 1.$$

We also have

$$w(\eta,\xi,t) = \exp\left(-\eta^2 t - \frac{1}{3}\xi^2 t\right), \qquad (\eta,\xi)\in\mathbb{R}^2,\ t\geq 0,$$

in the new variables, η and ξ.

3.2. The wavenumber regimes. We decompose $\mathbb{R}^2$ into suitable wavenumber regimes in η and ξ for some $0<q<1$ and $r>0$,

$$\Omega_1 := \left[-\Delta x^{q-1},\Delta x^{q-1}\right]\times\left[-\Delta x^{q-1},\Delta x^{q-1}\right], \tag{3.6}$$

$$\begin{aligned} \Omega_2 := \Big\{(\eta,\xi) :\ & -\Delta x^{q-1}\leq\xi\leq\Delta x^{q-1},\ -\frac{\pi}{\Delta x}+\xi\leq\eta\leq-\Delta x^{q-1}\\ & \vee\ \Delta x^{q-1}\leq\eta\leq\frac{\pi}{\Delta x}+\xi\Big\}, \end{aligned} \tag{3.7}$$

$$\begin{aligned} \Omega_3 := \Big\{(\eta,\xi) :\ & -\frac{\pi}{\Delta x}+\xi\leq\eta\leq\frac{\pi}{\Delta x}+\xi,\ -\Delta x^{-r}\leq\xi\leq-\Delta x^{q-1}\\ & \vee\ \Delta x^{q-1}\leq\xi\leq\Delta x^{-r}\Big\}, \end{aligned} \tag{3.8}$$

$$\Omega_4 := \mathbb{R}^2\backslash(\Omega_1\cup\Omega_2\cup\Omega_3), \tag{3.9}$$

which are also illustrated in Figure 2. By applying the inverse transforms to the error term we obtain an equation for the error in the (x,y)-plane for $t>0$, i.e.,

$$\begin{aligned} &(2\pi)^2(U(x,y,t)-u(x,y,t))\\ &\quad=\int_{-2t\Delta x^{-r}}^{2t\Delta x^{-r}}\int_{-\frac{\pi}{\Delta x}}^{\frac{\pi}{\Delta x}}(W(s,p,t)-w(s,p,t))\,\mathrm{e}^{-isx}\,\mathrm{e}^{-ipy}\,\mathrm{d}s\,\mathrm{d}p\\ &\qquad-\int_{\Omega_4}w(s,p,t)\,\mathrm{e}^{-isx}\,\mathrm{e}^{-ipy}\,\mathrm{d}s\,\mathrm{d}p\\ &\quad=\frac{2}{t}\int_{-\Delta x^{-r}}^{\Delta x^{-r}}\int_{-\frac{\pi}{\Delta x}+\xi}^{\frac{\pi}{\Delta x}+\xi}(W(\eta,\xi,t)-w(\eta,\xi,t))\,\mathrm{e}^{-i(\eta-\xi)x}\,\mathrm{e}^{-i\frac{2\xi y}{t}}\,\mathrm{d}\eta\,\mathrm{d}\xi\\ &\qquad-\frac{2}{t}\int_{\Omega_4}w(\eta,\xi,t)\,\mathrm{e}^{-i(\eta-\xi)x}\,\mathrm{e}^{-i\frac{2\xi y}{t}}\,\mathrm{d}\eta\,\mathrm{d}\xi. \end{aligned}$$

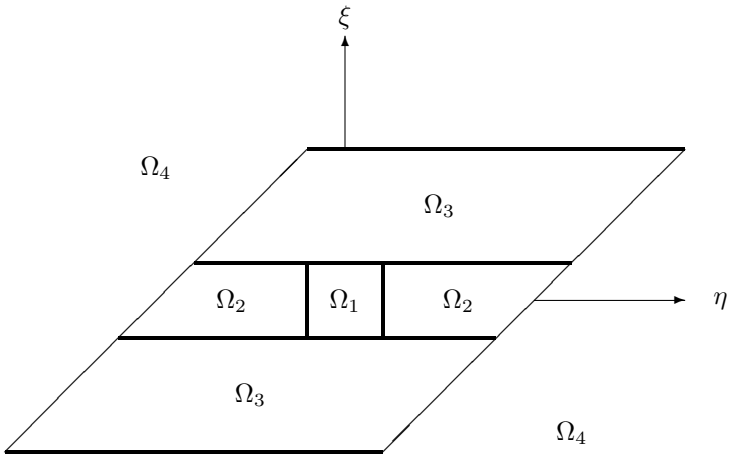

FIG. 2. *Schematic representation of the wavenumber regimes defined by* (3.6) *to* (3.9).

Here x is any x-grid node. We now define

$$I_1(x,y,t) := \int_{\Omega_1} (W(\eta,\xi,t) - w(\eta,\xi,t))\, \mathrm{e}^{-i(\eta-\xi)x}\, \mathrm{e}^{-i\frac{2\xi y}{t}}\, \mathrm{d}\eta\, \mathrm{d}\xi,$$
$$I_k(x,y,t) := \int_{\Omega_k} W(\eta,\xi,t)\, \mathrm{e}^{-i(\eta-\xi)x}\, \mathrm{e}^{-i\frac{2\xi y}{t}}\, \mathrm{d}\eta\, \mathrm{d}\xi, \qquad k=2,3,$$
$$I_4(x,y,t) := \int_{\mathbb{R}^2\setminus\Omega_1} w(\eta,\xi,t)\, \mathrm{e}^{-i(\eta-\xi)x}\, \mathrm{e}^{-i\frac{2\xi y}{t}}\, \mathrm{d}\eta\, \mathrm{d}\xi.$$

Except for the joint low wavenumber regime, we will perform separate calculations on W and w. We will find that all but the first term can be made exponentially small, while the first term is $O(\Delta x^2)$. We begin by considering the joint low wavenumber analysis for W and w.

3.3. Joint low wavenumbers (region Ω_1). We have to determine an exponent $q \in (0,1)$ such that, in Ω_1,

$$|\eta\Delta x| \le \Delta x^q \to 0 \qquad \text{and} \qquad |\xi\Delta x| \le \Delta x^q \to 0,$$

and certain expansions can be usefully truncated. By Taylor expansion,

$$-\frac{2t}{\Delta x^2}(1-\operatorname{sinc}(\xi\Delta x)\cos(\eta\Delta x)) = -\eta^2 t - \frac{1}{3}\xi^2 t + \frac{2t}{4!}\eta^4\Delta x^2 + \frac{2t}{5!}\xi^4\Delta x^2 + O\left(\eta^6\Delta x^4\right) + O\left(\xi^6\Delta x^4\right).$$

Our objective is to choose $q \in (0,1)$ so that the remainder terms, resulting from approximating the integrand of I_1 by its Taylor series expansion, are $o(\Delta x^2)$ as $\Delta x \to 0$. To this end, we write

$$\exp\left(\frac{2t}{4!}\eta^4\Delta x^2 + \frac{2t}{5!}\xi^4\Delta x^2 + o\left(\Delta x^2\right)\right) = 1 + \frac{2t}{4!}\eta^4\Delta x^2 + \frac{2t}{5!}\xi^4\Delta x^2 + o\left(\Delta x^2\right),$$

which is true if

$$\Delta x^4\left(\eta^8 + \xi^8\right) = o\left(\Delta x^2\right),$$

i.e., the second-order terms in the Taylor expansion of the exponential are negligible. We can therefore take $q \in (\frac{3}{4}, 1)$ to define the joint low wavenumber regime. Then,

$$
\begin{aligned}
I_1(x,y,t) &= \int_{\Omega_1} w \left(\exp\left(\frac{2t}{4!}\eta^4 \Delta x^2 + \frac{2t}{5!}\xi^4 \Delta x^2 + o\left(\Delta x^2\right)\right) - 1 \right) \mathrm{e}^{-i(\eta-\xi)x}\, \mathrm{e}^{-i\frac{2\xi y}{t}}\, \mathrm{d}\eta\, \mathrm{d}\xi \\
&= \int_{\Omega_1} w \left(\frac{2t}{4!}\eta^4 \Delta x^2 + \frac{2t}{5!}\xi^4 \Delta x^2 \right) \mathrm{e}^{-i(\eta-\xi)x}\, \mathrm{e}^{-i\frac{2\xi y}{t}}\, \mathrm{d}\eta\, \mathrm{d}\xi + o\left(\Delta x^2\right) \qquad (3.10) \\
&= \int_{\mathbb{R}^2} w \left(\frac{2t}{4!}\eta^4 \Delta x^2 + \frac{2t}{5!}\xi^4 \Delta x^2 \right) \mathrm{e}^{-i(\eta-\xi)x}\, \mathrm{e}^{-i\frac{2\xi y}{t}}\, \mathrm{d}\eta\, \mathrm{d}\xi + o\left(\Delta x^2\right) \\
&= \Delta x^2\, F(x,y,t) + o\left(\Delta x^2\right),
\end{aligned}
$$

where

$$
\begin{aligned}
F(x,y,t) &:= \int_{\mathbb{R}^2} w \left(\frac{2t}{4!}\eta^4 + \frac{2t}{5!}\xi^4 \right) \mathrm{e}^{-i(\eta-\xi)x}\, \mathrm{e}^{-i\frac{2\xi y}{t}}\, \mathrm{d}\eta\, \mathrm{d}\xi \\
&= \frac{t}{2} \int_{\mathbb{R}^2} w \left(\frac{2t}{4!}\left(s + \frac{pt}{2}\right)^4 + \frac{2t}{5!}\left(\frac{pt}{2}\right)^4 \right) \mathrm{e}^{-isx}\, \mathrm{e}^{-ipy}\, \mathrm{d}s\, \mathrm{d}p \\
&= t^2 \left(\frac{1}{4!}\left(\frac{\partial}{\partial x} + \frac{t}{2}\frac{\partial}{\partial y} \right)^4 + \frac{1}{5!}\left(\frac{t}{2}\frac{\partial}{\partial y} \right)^4 \right) u.
\end{aligned}
$$

We are able to replace Ω_1 by $\mathbb{R}^2$ in (3.10) to $o(\Delta x^2)$ because w decays exponentially in η and ξ (see also section 3.6). The last step uses the relation between the Fourier transform of a smooth function and the transforms of its derivatives.

Having dealt with the region Ω_1 in the (s,p)-plane, we move on to consider the remaining terms involving W. There are two cases to discuss, corresponding to low ξ-wavenumbers and high η-wavenumbers (region Ω_2) and to high ξ-wavenumbers (region Ω_3).

3.4. Low ξ-wavenumbers and high η-wavenumbers (region Ω_2). For these wavenumbers we have $\eta\Delta x \in [-\pi + \xi\Delta x, \pi + \xi\Delta x]$ and in this interval $\eta = 0$ is the only solution to $\cos(\eta\Delta x) = 1$ since $|\xi\Delta x| \le \Delta x^q$. The following inequality is valid for $\theta \in [-\pi, \pi]$:

$$
\sin^2\left(\frac{\theta}{2}\right) \ge \left(\frac{\theta}{\pi}\right)^2.
$$

However since we wish to take $\theta = \eta\Delta x$ with $\theta \in [-\pi + \xi\Delta x, \pi + \xi\Delta x]$ and $|\xi\Delta x| \le \Delta x^q$, we shall use instead the weaker inequality

$$
\sin^2\left(\frac{\theta}{2}\right) \ge \frac{1}{4}\left(\frac{\theta}{\pi}\right)^2,
$$

which is valid for all such θ, provided that Δx is sufficiently small (whereby also $|\xi\Delta x| \le \Delta x^q$ is sufficiently small). Hence,

$$
\cos(\eta\Delta x) = 1 - 2\sin^2\left(\frac{\eta\Delta x}{2}\right) \le 1 - \frac{1}{2}\left(\frac{\eta\Delta x}{\pi}\right)^2 = 1 - \frac{1}{2\pi^2}(\eta\Delta x)^2.
$$

We can then choose $\alpha < \frac{1}{2\pi^2}$ such that for small enough Δx we have

$$
\cos(\eta\Delta x) \le 1 - \alpha(\eta\Delta x)^2
$$

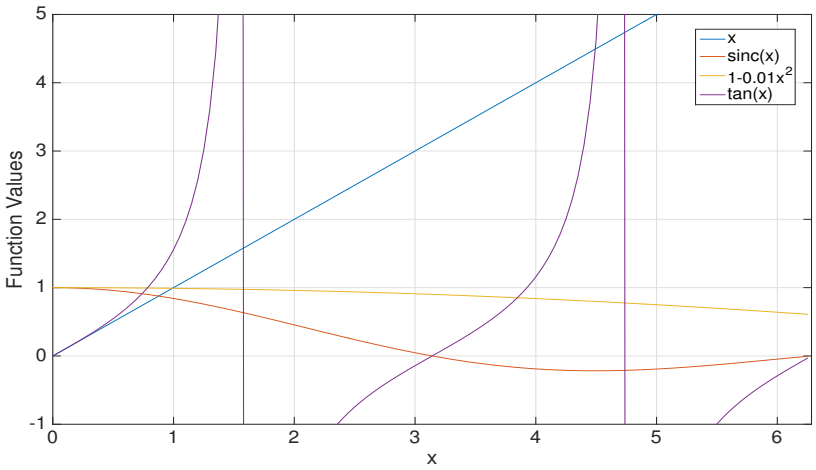

FIG. 3. *Plot of* $\operatorname{sinc} x = \frac{\sin x}{x}$ *and its relation to other functions needed in section* 3.5.

for $\eta\Delta x \in [-\pi + \xi\Delta x, \pi + \xi\Delta x]$, since $|\xi\Delta x| \le \Delta x^q \to 0$ as $\Delta x \to 0$. Also, for $\xi\Delta x$ small enough, we can ensure that

$$\frac{1}{2} < \operatorname{sinc}(\xi\Delta x) \le 1.$$

So then, for $\cos(\eta\Delta x) \ge 0$,

$$\alpha(\eta\Delta x)^2 \le 1 - \operatorname{sinc}(\xi\Delta x)\cos(\eta\Delta x). \tag{3.11}$$

If, on the other hand, $\cos(\eta\Delta x) \le 0$, then, because we always have $\alpha(\eta\Delta x)^2 \le \frac{1}{2\pi^2}(\pi + \Delta x^q)^2 \le 1$ for Δx sufficiently small (more precisely, for $\Delta x \le [(\sqrt{2}-1)\pi]^{1/q}$), while the right-hand side of (3.11) is ≥ 1 for $\cos(\eta\Delta x) \le 0$, it once again follows that (3.11) holds. Hence,

$$\exp\left(-\frac{2t}{\Delta x^2}(1 - \operatorname{sinc}(\xi\Delta x)\cos(\eta\Delta x))\right) \le \exp\left(-\frac{2t}{\Delta x^2}\alpha(\eta\Delta x)^2\right) \le \exp\left(-2\alpha t \Delta x^{2(q-1)}\right)$$

as $\eta\Delta x \ge \Delta x^q$ and $\eta^2 \ge \Delta x^{2(q-1)}$. Thus, the contribution to the integral satisfies

$$|I_2| \le \int_{\Omega_2} W(\eta,\xi,t)\,\mathrm{d}\eta\,\mathrm{d}\xi = o(\Delta x^m) \qquad \text{as } \Delta x \to 0$$

for all $m > 0$.

3.5. High ξ-wavenumbers (region Ω_3). We observe that $\xi \mapsto \operatorname{sinc}(\xi\Delta x)$ is a decreasing function of $\xi \in [0,\infty)$ from 0 from $\xi = \Delta x^{q-1}$ to some $\xi = \xi_0$ if we make Δx small enough. At that first local minimum, ξ_0, one then has $\tan(\xi_0\Delta x) = \xi_0\Delta x$ and then $|\operatorname{sinc}(\xi_0\Delta x)| = \alpha$ with $\alpha < 0.3$, say, and for values of $\xi > \xi_0$, we have $|\operatorname{sinc}(\xi\Delta x)| < \alpha$. This is illustrated in Figure 3, with the symbol $\times$ in the figure signifying $\xi\Delta x$.

We see that for $0 < \xi \le \xi_0$ we also have (see again Figure 3)

$$\operatorname{sinc}(\xi\Delta x)\cos(\eta\Delta x) \le |\operatorname{sinc}(\xi\Delta x)| < 1 - \frac{1}{100}(\xi\Delta x)^2,$$

while for $\xi \geq \xi_0$ we have

$$\operatorname{sinc}(\xi\Delta x)\cos(\eta\Delta x) \leq |\operatorname{sinc}(\xi\Delta x)| \leq \alpha\,(<0.3).$$

So, for $\xi\Delta x \geq \Delta x^q$, the following inequality holds:

$$1-\operatorname{sinc}(\xi\Delta x)\cos(\eta\Delta x) \geq \frac{1}{100}\min\big(\Delta x^{2q}, 100(1-\alpha)\big).$$

Therefore,

$$\begin{aligned}\exp\left(-\frac{2t}{\Delta x^2}(1-\operatorname{sinc}(\xi\Delta x)\cos(\eta\Delta x))\right) &\leq \exp\left(-\frac{t}{50\Delta x^2}\min(\Delta x^{2q}, 100(1-\alpha))\right)\\ &\leq \exp\left(-\frac{t}{50\Delta x^{2(1-q)}}\right)\end{aligned}$$

for small enough Δx. Hence, similarly as before (cf. section 3.4),

$$|I_3| \leq (2\Delta x^{-r})(2\pi\Delta x^{-1})\exp\left(-\frac{t}{50}\Delta x^{-2(1-q)}\right) = o(\Delta x^m) \qquad \text{as } \Delta x \to 0$$

for all $m > 0$.

Remark 2. We note that for the high ξ-wavenumber integration range to be nonempty, we need that

$$\Delta x^{q-1} < \Delta x^{-r},$$

i.e., $r > 1-q$. If $r \leq 1-q$, there is only a low ξ-wavenumber regime, but this is irrelevant for the computations, and quadratic convergence is still guaranteed for any $r \in (0,1)$ because the contributions from outside $(-\Delta x^{-r}, \Delta x^{-r})$ decay exponentially for all r as $\Delta x \to 0$.

Remark 3. For any fixed Δx, the numerical double Fourier transform W in (3.5) approaches a constant value of $\exp(-2t/\Delta x^2)$ as $\xi \to \pm\infty$ (equivalently, $p \to \pm\infty$) independent of η (or s); hence,

$$\lim_{p\to\pm\infty} V_j(p,t) = \lim_{p\to\pm\infty}\frac{1}{2\pi}\int_{-\frac{\pi}{\Delta x}}^{\frac{\pi}{\Delta x}} W(s,p,t)\,\mathrm{e}^{isx_j}\,\mathrm{d}s = \begin{cases}\frac{1}{\Delta x}\exp(-2t/\Delta x^2) & \text{if } j=0,\\ 0 & \text{if } j\neq 0.\end{cases}$$

This implies that for $j=0$, the integrand appearing in (2.1), as a function of p, does not belong to $L^1(\mathbb{R})$, which is yet another reason why instead of using the actual inverse Fourier transform in (2.1) to define $U(x_j,y,t)$ with $\mathbb{R}$ as the integration range, we have integrated over the compact interval $[-2t\Delta x^{-r}, 2t\Delta x^{-r}]$. For $t>0$ the sequence of integrals converges to the true inverse Fourier transform as $\Delta x \to 0$, because $V_0(p,t)$ decays to zero exponentially fast with $\Delta x \to 0$ for any given, large enough, p.

3.6. Localization of the exact Fourier transform (region Ω_4). Finally, we need to estimate the error contribution for the remaining terms, which involve w. We get

$$\begin{aligned}|I_4| \;\leq\; &\int_{-\infty}^{\infty}\int_{-\infty}^{-\Delta x^{q-1}} w\;\mathrm{d}\eta\,\mathrm{d}\xi + \int_{-\infty}^{\infty}\int_{\Delta x^{q-1}}^{\infty} w\;\mathrm{d}\eta\,\mathrm{d}\xi\\ &+\int_{\Delta x^{q-1}}^{\infty}\int_{-\infty}^{\infty} w\;\mathrm{d}\eta\,\mathrm{d}\xi + \int_{-\infty}^{-\Delta x^{q-1}}\int_{-\infty}^{\infty} w\;\mathrm{d}\eta\,\mathrm{d}\xi.\end{aligned}$$

As we have for any $t > 0$

$$\int_{-\infty}^{\infty} w(\eta,\xi,t)\,\mathrm{d}\eta = \exp\Big(-\frac{1}{3}t\xi^2\Big)\int_{-\infty}^{\infty}\exp\left(-t\eta^2\right)\mathrm{d}\eta = \sqrt{\frac{\pi}{t}}\exp\Big(-\frac{1}{3}t\xi^2\Big)$$

and

$$\int_{-\infty}^{\infty} w(\eta,\xi,t)\,\mathrm{d}\xi = \exp\left(-t\eta^2\right)\int_{-\infty}^{\infty}\exp\Big(-\frac{1}{3}t\xi^2\Big)\,\mathrm{d}\xi = \sqrt{\frac{3\pi}{t}}\exp\left(-t\eta^2\right),$$

it follows that

$$\begin{aligned}|I_4| \le{}& \sqrt{\frac{3\pi}{t}}\int_{-\infty}^{-\Delta x^{q-1}}\exp\left(-t\eta^2\right)\mathrm{d}\eta + \sqrt{\frac{3\pi}{t}}\int_{\Delta x^{q-1}}^{\infty}\exp\left(-t\eta^2\right)\mathrm{d}\eta\\ &+\sqrt{\frac{\pi}{t}}\int_{\Delta x^{q-1}}^{\infty}\exp\Big(-\frac{1}{3}t\xi^2\Big)\,\mathrm{d}\xi + \sqrt{\frac{\pi}{t}}\int_{-\infty}^{-\Delta x^{q-1}}\exp\Big(-\frac{1}{3}t\xi^2\Big)\,\mathrm{d}\xi.\end{aligned}$$

Lemma 3 in the appendix of [5] implies that for any $t > 0$ each of these integrals is $o(\Delta x^m)$, for any $m > 0$.

Collecting the above results we find that

$$\begin{aligned}U(x,y,t) - u(x,y,t) &= \frac{1}{2t\pi^2}\left(I_1(x,y,t) + I_2 + I_3 - I_4\right)\\ &= \frac{1}{2t\pi^2}\left(I_1(x,y,t) + o(\Delta x^m)\right)\\ &= \Delta x^2\left[\frac{t}{2\pi^2}\left(\frac{1}{4!}\left(\frac{\partial}{\partial x}+\frac{t}{2}\frac{\partial}{\partial y}\right)^4 + \frac{1}{5!}\left(\frac{t}{2}\frac{\partial}{\partial y}\right)^4\right)u\right]\Bigg|_{(x,y,t)}\\ &\quad + o\left(\Delta x^2\right)\quad \text{as } \Delta x \to 0,\end{aligned}$$

which completes the proof of Theorem 3.1.

4. Multidimensional problems. It is straightforward to extend the toy model (1.4), (1.5) to higher dimensions by introducing multiple diffusive terms or multiple drift terms. We present the analysis for the semidiscretization of an equation with two diffusive dimensions in the remainder of this section. We do not envisage any substantial difficulties for extensions to three or more such dimensions, but, as will be visible from the analysis below, writing out the derivation for the general case will be exceedingly lengthy, without contributing any new insights.

4.1. Multiple diffusive terms. We consider the case of a PDE with a single drift coefficient which is a linear combination of the components of x,

(4.1)
$$\begin{aligned}\frac{\partial u}{\partial t} + (\gamma_1 x_1 + \gamma_2 x_2)\frac{\partial u}{\partial y} &= a_{11}\frac{\partial^2 u}{\partial x_1^2} + 2a_{12}\frac{\partial^2 u}{\partial x_1 \partial x_2} + a_{22}\frac{\partial^2 u}{\partial x_2^2}, (x_1,x_2,y,t) \in \mathbb{R}^3 \times (0,T],\\ u(x_1,x_2,y,0) &= \delta(x_1 - x_{1,0}) \otimes \delta(x_2 - x_{2,0}) \otimes \delta(y - y_0), \qquad (x_1,x_2,y) \in \mathbb{R}^3,\end{aligned}$$

which extends the toy model to one containing two independent variables x_1 and x_2. We consider the hypoelliptic case, i.e., where $(\gamma_1,\gamma_2) \neq (0,0)$ and $(a_{ij})_{1\le i,j,\le 2}$ is strictly positive definite, i.e., $a_{11}, a_{22} > 0$ and $a_{11}a_{22} > a_{12}^2$.

We apply the y-FT to get

(4.2)
$$\frac{\partial v}{\partial t} - ip(\gamma_1 x_1 + \gamma_2 x_2)v = a_{11}\frac{\partial^2 v}{\partial x_1^2} + 2a_{12}\frac{\partial^2 v}{\partial x_1 \partial x_2} + a_{22}\frac{\partial^2 v}{\partial x_2^2}, \quad (x_1, x_2, p, t) \in \mathbb{R}^3 \times (0, T].$$

For the analytical solution we next apply the x_1-FT and the x_2-FT in turn to get

(4.3)
$$\frac{\partial w}{\partial t} - p\left(\gamma_1 \frac{\partial w}{\partial s_1} + \gamma_2 \frac{\partial w}{\partial s_2}\right) = -\left(a_{11}s_1^2 + 2a_{12}s_1 s_2 + a_{22}s_2^2\right) w, \quad (s_1, s_2, p, t) \in \mathbb{R}^3 \times (0, T],$$

in conjunction with the initial condition $w(s_1, s_2, p, 0) = 1$. We now make an ansatz

$$w(s_1, s_2, p, t) = \exp\left(-a_{11}s_1^2 t - 2a_{12}s_1 s_2 t - a_{22}s_2^2 t - B_1 s_1 p t^2 - B_2 s_2 p t^2 - C p^2 t^3\right),$$

and by insertion we get

$$B_1 = \gamma_1 a_{11} + \gamma_2 a_{12}, \quad B_2 = \gamma_1 a_{12} + \gamma_2 a_{22}, \quad C = \frac{1}{3}(\gamma_1(a_{11} + a_{12}) + \gamma_2(a_{12} + a_{22})),$$

and thus we have the analytical solution in Fourier space. We could, if necessary, invert all these transforms, but we will instead concentrate on the effect of discretization in the x_1- and x_2-directions. So we now start with the PDE (4.2) and discretize this by

$$\begin{aligned}
&\frac{\partial V_{j,k}}{\partial t} - ip(\gamma_1 x_{1,j} + \gamma_2 x_{2,k})V_{j,k} \\
&\quad = a_{11}\frac{V_{j+1,k} - 2V_{j,k} + V_{j-1,k}}{\Delta x_1^2} \\
&\qquad + 2a_{12}\frac{V_{j+1,k+1} - V_{j+1,k-1} - V_{j-1,k+1} + V_{j-1,k-1}}{4\Delta x_1 \Delta x_2} + a_{22}\frac{V_{j,k+1} - 2V_{j,k} + V_{j,k-1}}{\Delta x_2^2},
\end{aligned}$$

where we have omitted p and t as arguments for the sake of brevity, and where $V_{j,k}(p, t)$ is an approximation to $v(x_{1,j}, x_{2,k}, p, t)$ on a uniform two-dimensional mesh of spacings $\Delta x_1, \Delta x_2 > 0$.

For the sake of simplicity of the exposition, we restrict ourselves to the special case $\gamma_1 = 1$, $\gamma_2 = 0$, $a_{11} = a_{22} = 1$, $a_{12} = \rho \in (-1, 1)$, i.e., we consider

$$\frac{\partial u}{\partial t} + x_1 \frac{\partial u}{\partial y} = \frac{\partial^2 u}{\partial x_1^2} + 2\rho\frac{\partial^2 u}{\partial x_1 \partial x_2} + \frac{\partial^2 u}{\partial x_2^2}. \tag{4.4}$$

Remark 4. Equation (4.4) is a simplified case of the general equation (4.1), where the term x_2 has been dropped from the drift and the diffusion is normalized. This can be achieved by a rotation of the original co-ordinates to align the drift (γ_1, γ_2) with the x_1-axis and by subsequent scaling of the new y, x_1, and x_2 co-ordinates.

We can then apply the Fourier transforms in the x_1 and x_2 variables and after steps similar to the one-dimensional case obtain the solution for the double-transformed equation,

$$W(s_1, s_2, p, t) = w(s_1, s_2, p, t) \exp\left(\frac{1}{p}\int_{s_1}^{s_1 + pt} (g_{11}(\sigma, s_2) + 2\rho g_{12}(\sigma, s_2) + g_{22}(\sigma, s_2))\, \mathrm{d}\sigma\right),$$

where

$$g_{11}(s_1,s_2) = s_1^2 - \frac{4}{\Delta x_1^2}\sin^2\left(\frac{s_1\Delta x_1}{2}\right), \qquad g_{22}(s_1,s_2) \quad = s_2^2 - \frac{4}{\Delta x_2^2}\sin^2\left(\frac{s_2\Delta x_2}{2}\right),$$
$$g_{12}(s_1,s_2) = s_1 s_2 - \frac{1}{\Delta x_1 \Delta x_2}\sin\left(s_1\Delta x_1\right)\sin\left(s_2\Delta x_2\right).$$

We can now investigate the low and high wavenumber behavior in terms of the new variables. Similarly to the one-dimensional case, by standard integration and the change of variables $\xi = pt/2$ and $\eta_1 = s_1 + pt/2$ we find

$$W(\eta_1,s_2,\xi,t) = W_1(\eta_1,\xi,t)\,W_{12}(\eta_1,s_2,\xi,t)\,W_2(s_2,t),$$

where

$$W_1(\eta_1,\xi,t) = \exp\left(-\frac{2t}{\Delta x_1^2}\left(1-\operatorname{sinc}(\xi\Delta x_1)\cos(\eta_1\Delta x_1)\right)\right)$$

is the solution from the one-dimensional case and

$$W_{12}(\eta_1,s_2,\xi,t) = \exp\left(-2t\rho\operatorname{sinc}(\xi\Delta x_1)\frac{\sin(\eta_1\Delta x_1)}{\Delta x_1}\frac{\sin(s_2\Delta x_2)}{\Delta x_2}\right),$$
$$W_2(s_2,t) = \exp\left(-\frac{4t}{\Delta x_2^2}\sin^2(s_2\Delta x_2/2)\right).$$

The exact solution in these variables is

$$w(\eta_1,s_2,\xi,t) = \exp\left(-t\left\{\eta_1^2 + \frac{\xi^2}{3} + s_2^2 + 2\rho\eta_1 s_2\right\}\right), \tag{4.5}$$

and we recognize in the first two terms the one-dimensional solution

$$w_1(\eta_1,\xi,t) = \exp\left(-t\left\{\eta_1^2 + \frac{\xi^2}{3}\right\}\right). \tag{4.6}$$

We proceed by a wavenumber analysis broadly similar to the one before, but made more complicated by the presence of an extra variable s_2 and the fact that the problem degenerates as $|\rho| \to 1$, necessitating a more careful estimation for ρ close to 1.

4.2. Joint low wavenumbers. We write

$$\log W = \log W_1 - t\left\{2\rho\operatorname{sinc}(\xi\Delta x_1)\frac{\sin(\eta_1\Delta x_1)}{\Delta x_1}\frac{\sin\left(s_2\Delta x_2\right)}{\Delta x_2} + \frac{4}{\Delta x_2^2}\sin^2\left(\frac{s_2\Delta x_2}{2}\right)\right\}$$

and compare this to

$$\log w = \log w_1 - t\{s_2^2 + 2\rho\eta_1 s_2\},$$

where w is the exact solution to the two-dimensional problem from (4.5) and w_1 is the solution to the one-dimensional problem from (4.6). By standard Taylor expansion we find, with $\doteq$ denoting "up to terms $o(\Delta x_1^2) + o(\Delta x_2^2)$,"

$$\log(W/w) \doteq \log(W_1/w_1) + 2\rho t\left(\frac{1}{12}\eta_1 s_2^3\Delta x_2^2 + \frac{1}{6}\eta_1^3 s_2^2\Delta x_1^2 + \eta_1 s_2^2\xi^2\Delta x_1^2\right) + \frac{t}{12}s_2^4\Delta x_2^2$$
$$\doteq \left(\frac{2t}{4!}\eta_1^4 + \frac{2t}{5!}\xi^4 + \frac{\rho t}{3}\eta_1^3 s_2^2 + 2\rho t\eta_1 s_2^2\xi^2\right)\Delta x_1^2 + \left(\frac{\rho t}{6}\eta_1 s_2^3 + \frac{t}{12}s_2^4\right)\Delta x_2^2.$$

Therefore the numerical error contribution from the low wavenumber regime is

(4.7)
$$I_1(x_1,x_2,y,t) = \Delta x_1^2 F_1(x_1,x_2,y,t) + \Delta x_2^2 F_2(x_1,x_2,y,t) + o\left(\Delta x_1^2\right) + o\left(\Delta x_2^2\right),$$

where, denoting $D_1 = \frac{\partial}{\partial x_1} + \frac{t}{2}\frac{\partial}{\partial y}$,

$$F_1 = t^2\left(\frac{1}{4!}D_1^4 + \frac{1}{5!}\left(\frac{t}{2}\frac{\partial}{\partial y}\right)^4\right)u + \ t^2\left(\frac{\rho}{3!}D_1^3\frac{\partial^2}{\partial x_2^2} + \rho D_1\frac{\partial^2}{\partial x_2^2}\left(\frac{t}{2}\frac{\partial}{\partial y}\right)^2\right)u,$$
$$F_2 = t^2\left(\frac{2\rho}{4!}\left(\frac{\partial}{\partial x_1} + \frac{t}{2}\frac{\partial}{\partial y}\right)\frac{\partial^3}{\partial x_2^3} + \frac{1}{4!}\frac{\partial^4}{\partial x_2^4}\right)u.$$

The point is less the explicit form, but rather that the error can be expressed in terms of up to fifth mixed partial derivatives, or up to fourth if $\rho = 0$. As in section 3, we will find that this is the only wavenumber range that contributes to the leading-order error, and therefore (4.7) describes the discretization error up to higher-order terms.

4.3. Low ξ-wavenumbers and high η_1- or s_2-wavenumbers. We require two simple inequalities. The first one states that for $|\eta_1\Delta x_1| \le \pi/2$, and since $\operatorname{sinc}(\xi\Delta x_1) > 0$ (in the present small ξ regime),

$$1 - \operatorname{sinc}(\xi\Delta x_1)\cos(\eta_1\Delta x_1) \ge 1 - \cos(\eta_1\Delta x_1) = 2\sin^2(\eta_1\Delta x_1/2).$$

The second elementary inequality used in the argument below, in the transition from the second-to-last inequality to the last inequality, is that

$$\sin\alpha \ge \frac{2}{\pi}\alpha \qquad \text{for} \qquad 0 \le \alpha \le \frac{\pi}{2}.$$

Therefore, dropping the t in the argument for brevity, for $|\eta_1\Delta x_1| \le \pi/2$,

$$\begin{aligned}
&W(\eta_1,s_2)\\
&\quad\le \exp\left(-\frac{4t}{\Delta x_1^2}\sin^2(\eta_1\Delta x_1/2) + 2t|\rho|\frac{|\sin(\eta_1\Delta x_1)|}{\Delta x_1}\frac{|\sin(s_2\Delta x_2)|}{\Delta x_2}\right)\cdot W_2(s_2)\\
&\quad\le \exp\left(-\frac{4t}{\Delta x_1^2}\sin^2(\eta_1\Delta x_1/2) + 8t|\rho|\frac{|\sin(\eta_1\Delta x_1/2)|}{\Delta x_1}\frac{|\sin(s_2\Delta x_2/2)|}{\Delta x_2}\right)\cdot W_2(s_2)\\
&\quad= \exp\left(-4t(1-|\rho|)\left(\frac{1}{\Delta x_1^2}\sin^2(\eta_1\Delta x_1/2) + \frac{1}{\Delta x_2^2}\sin^2(s_2\Delta x_2/2)\right)\right)\\
&\qquad\cdot \exp\left(-4t|\rho|\left(\frac{\sin(\eta_1\Delta x_1/2)}{\Delta x_1} - \frac{\sin^2(s_2\Delta x_2)}{\Delta x_2}\right)^2\right)\\
&\quad\le \exp\left(-4t(1-|\rho|)\left(\frac{1}{\Delta x_1^2}\sin^2(\eta_1\Delta x_1/2) + \frac{1}{\Delta x_2^2}\sin^2(s_2\Delta x_2/2)\right)\right)\\
&\quad\le \exp\left(-\frac{4\,t\,(1-|\rho|)}{\pi^2}\left(\eta_1^2+s_2^2\right)\right)\\
&= o(\Delta x^r) \qquad \text{as } \Delta x \to 0
\end{aligned}$$

for any $r > 0$ if either $\nu_1 \ge \Delta x_1^{-q}$ or $s_2 \ge \Delta x_2^{-q}$ for any $q > 0$.

For $|\eta_1\Delta x_1| > \pi/2$, we have that

$$1 - \operatorname{sinc}(\xi\Delta x_1)\cos(\eta_1\Delta x_1) \ge 1,$$

and therefore

$$\begin{aligned}
W(\eta_1,s_2) &\le \exp\left(-\frac{2t}{\Delta x_1^2}+2t|\rho|\frac{1}{\Delta x_1}\frac{|\sin(s_2\Delta x_2)|}{\Delta x_2}-\frac{4t}{\Delta x_2^2}\sin^2(s_2\Delta x_2/2)\right)\\
&\le \exp\left(-\frac{2t}{\Delta x_1^2}+\frac{4t}{\Delta x_1}\frac{|\sin(s_2\Delta x_2/2)|}{\Delta x_2}-\frac{4t}{\Delta x_2^2}\sin^2(s_2\Delta x_2/2)\right)\\
&\le \exp\left(-\frac{2t}{\Delta x_1^2}+\frac{\sqrt{21}t}{\Delta x_1}\frac{|\sin(s_2\Delta x_2/2)|}{\Delta x_2}-\frac{4t}{\Delta x_2^2}\sin^2(s_2\Delta x_2/2)\right)\\
&= \exp\left(-\frac{t}{2}\left(\frac{1}{\Delta x_1^2}+\frac{1}{\Delta x_2^2}\sin^2(s_2\Delta x_2/2)\right)\right)\\
&\quad\cdot\exp\left(-t\left(\sqrt{\frac{3}{2}}\frac{1}{\Delta x_1}-\sqrt{\frac{7}{2}}\frac{|\sin(s_2\Delta x_2/2)|}{\Delta x_2}\right)^2\right)\\
&\le \exp\left(-\frac{t}{2}\left(\frac{1}{\Delta x_1^2}+\frac{1}{\Delta x_2^2}\sin^2(s_2\Delta x_2/2)\right)\right)\\
&= o(\Delta x^r)
\end{aligned}$$

as before.

4.4. High ξ-wavenumbers. Completing squares, we write

$$\begin{aligned}
&W(\eta_1,s_2,\xi)\\
&= W_1(\eta_1,\xi)\cdot\exp\left(\frac{t}{\Delta x_1^2}\cos^2(s_2\Delta x_2/2)\operatorname{sinc}^2(\xi\Delta x_1)\sin^2(\eta_1\Delta x_1)\rho^2\right)\\
&\quad\cdot\exp\left(-t\left(\frac{\rho}{\Delta x_1}\cos(s_2\Delta x_2/2)\operatorname{sinc}(\xi\Delta x_1)\sin(\eta_1\Delta x_1)+\frac{2}{\Delta x_2}\sin(s_2\Delta x_2/2)\right)^2\right),
\end{aligned}$$

and so, neglecting the last factor, which is ≤ 1,

$$\begin{aligned}
\log W &\le \log W_1(\eta_1,\xi)+\rho^2\frac{t}{\Delta x_1^2}\cos^2(s_2\Delta x_2/2)\operatorname{sinc}^2(\xi\Delta x_1)\sin^2(\eta_1\Delta x_1)\\
&\le \frac{t}{\Delta x_1^2}\left(-2+2\operatorname{sinc}(\xi\Delta x_1)\cos(\eta_1\Delta x_1)+\operatorname{sinc}^2(\xi\Delta x_1)\sin^2(\eta_1\Delta x_1)\right)\\
&\le \frac{t}{\Delta x_1^2}\left(-2+|\operatorname{sinc}(\xi\Delta x_1)|\left(2|\cos(\eta_1\Delta x_1)|+\sin^2(\eta_1\Delta x_1)\right)\right)\\
&= \frac{t}{\Delta x_1^2}\left(-2+|\operatorname{sinc}(\xi\Delta x_1)|\left(2-(1-|\cos(\eta_1\Delta x_1)|)^2\right)\right)\\
&\le -\frac{2t}{\Delta x_1^2}(1-|\operatorname{sinc}(\xi\Delta x_1)|).
\end{aligned}$$

Following the remainder of the argument in the one-dimensional case we can deduce that the contribution from this range is also exponentially small.

4.5. Multiple drift terms. Another possible extension is a model of the form

$$\frac{\partial u}{\partial t}+a_1x\frac{\partial u}{\partial y_1}+a_2x\frac{\partial u}{\partial y_2}=\frac{\partial^2 u}{\partial x^2}, \tag{4.8}$$

where $(a_1,a_2)\neq(0,0)$ so that we have two drift terms and neither of the drift coefficients depend on y. For this, we can apply the y_1-FT and the y_2-FT to get

$$\frac{\partial v}{\partial t}-ia_1p_1xv-ia_2p_2xv=\frac{\partial^2 v}{\partial x^2},$$

where p_1 and p_2 are wavenumbers. To find the analytical solution we apply the x-FT to get

$$\frac{\partial w}{\partial t} - (a_1 p_1 + a_2 p_2)\frac{\partial w}{\partial s} = -s^2 w.$$

The analysis would then continue as before but with $a_1p_1+a_2p_2$ as a joint wavenumber. In this situation, however, the wavenumbers have to be handled differently. For example, we can have separately large values of $|p_1|$ and $|p_2|$, but the value of $a_1p_1 + a_2p_2$ can be small.

5. Computation of the semidiscrete Fourier solution. In this section we present the results of applying the semidiscrete Fourier scheme to the toy model (1.4), (1.5). We compute the solution to (2.5), (2.6) by using the matrix exponential and we then use the trapezium rule and the FFT to compute the values of $U(x_j, y_k, T)$ from (2.1).

5.1. Solving the ODEs. The ODE system (2.5) can be written as

$$\frac{\mathrm{d}}{\mathrm{d}t}V(p,t) = MV(p,t), \tag{5.1}$$

where $V = (V_j)_j$ is an infinite column-vector and $M = M_1 + ipM_2$ is a bi-infinite matrix with

$$M_1 = \frac{1}{\Delta x^2}\begin{pmatrix} \dots & \dots & \dots & \dots & \dots & \dots & \dots \\ \dots & -2 & 1 & 0 & 0 & 0 & \dots \\ \dots & 1 & -2 & 1 & 0 & 0 & \dots \\ \dots & 0 & 1 & -2 & 1 & 0 & \dots \\ \dots & 0 & 0 & 1 & -2 & 1 & \dots \\ \dots & 0 & 0 & 0 & 1 & -2 & \dots \\ \dots & \dots & \dots & \dots & \dots & \dots & \dots \end{pmatrix}, \qquad M_2 = \Delta x \begin{pmatrix} \dots & \dots & \dots & \dots & \dots & \dots & \dots \\ \dots & -2 & 0 & 0 & 0 & 0 & \dots \\ \dots & 0 & -1 & 0 & 0 & 0 & \dots \\ \dots & 0 & 0 & 0 & 0 & 0 & \dots \\ \dots & 0 & 0 & 0 & 1 & 0 & \dots \\ \dots & 0 & 0 & 0 & 0 & 2 & \dots \\ \dots & \dots & \dots & \dots & \dots & \dots & \dots \end{pmatrix}.$$

In our implementation, the problem is considered over a sufficiently large interval $x \in (-L, L)$ with homogeneous Dirichlet boundary condition at $x = \pm L$; in the numerical experiments below we took $L = 10$ or $L = 20$ to ensure that the Dirichlet boundary condition has negligible influence on the values of the numerical solution at the final time of interest, $T > 0$. Hence, the bi-infinite matrices M_1, M_2, and M are truncated to square matrices $\widetilde{M}_1$, $\widetilde{M}_2$, and $\widetilde{M}$ of a certain finite size (depending on the choice of L and Δx). Since the matrix $\widetilde{M}$ is independent of t, the truncated counterpart of (5.1) has the obvious solution

$$\widetilde{V}(p,t) = V(p,0)\,\mathrm{e}^{\widetilde{M}t}, \qquad p \in \mathbb{R},\ t > 0, \tag{5.2}$$

where $V_j(p,0) = 0$ for $j \neq 0$ and $V_0(p,0) = \frac{1}{\Delta x}$.

In our numerical experiments we used the MATLAB `expm` function for the matrix exponential, which is based on the scaling and squaring method (cf. [6]). The exact solution (5.2) in the form of a matrix exponential is only available because the coefficients of (1.4) do not depend on time. The solution of (5.1) can, in principle, be found for any value of p, but in practice we will only be able to calculate a finite number of values, $\widetilde{V}_j(p_k, T)$. To compute the solution in the original variables, we numerically invert the y-FT, using the grid values, $\widetilde{V}_j(p_k, T)$. By using this method, we have avoided discretizing the y-partial derivative: in effect, this is replaced by a discretization in the p-direction. As an alternative to matrix exponentiation, we present in section 5.5 the results obtained by a numerical method based on time stepping.

5.2. Convergence of the p-discretization. When we solve the Kolmogorov forward equation using the semidiscrete Fourier method, we need to consider the effect of the numerical inversion of the y-FT in the final step of the solution procedure. As the inversion is only approximate, we have to decide how to set the parameters for the inversion, and, more specifically, how to choose the range of p-wavenumbers and the p-step.

According to the Euler–Maclaurin expansion, the error of the composite trapezium rule applied to a sufficiently smooth function f over an interval $[a,b]$ can be expressed as follows (see, for example, [15, Theorem 7.4, pp. 213]:

$$\sum_{j=1}^{k} c_j h^{2j}\left[f^{(2k-1)}(b)-f^{(2k-1)}(a)\right]-\left(\frac{h}{2}\right)^{2k}\int_a^b q_{2k}(\tau(p))f^{(2k)}(p)\,\mathrm{d}p, \tag{5.3}$$

where $h=(b-a)/m$ is the uniform grid size, τ is a piecewise linear "saw tooth" function with values in $[-1,1]$, and q_{2k} and c_j, $j=1,\dots,k$ are computable polynomials and constants, respectively.

The integrand in (2.1), up to a p-integrable $O(h^2)$ term, is, for x, y, and t fixed,

$$f(p)=V(x,p,t)\exp(-ipy)=\frac{1}{2\sqrt{\pi t}}\exp\left(-\frac{t^3}{12}p^2+i\frac{xt}{2}p-\frac{x^2}{4t}\right)\exp(-ipy), \tag{5.4}$$

as one finds by taking the inverse Fourier transform (in s) of (3.4).

In our case, the integrand (5.4) and its derivatives (in p) vanish so rapidly for large p that by taking the integration limits to be $a=-2t\Delta x^{-r}$ and $b=2t\Delta x^{-r}$ the first term in (5.3) becomes exponentially small in Δx for any fixed k. Then, taking $m=n_p:=l_{\max}-l_{\min}+1$ in (2.2) such that $h=\Delta p=4t\Delta x^{-r}/n_p\to 0$, say, $h=\Delta x^r$, the second term is $O(h^{2k})$ for any k. Hence, the total error can be made exponentially small in Δx. See [17] for a detailed discussion of the behavior of the trapezium rule for analytic integrands in a neighborhood of the real line.

5.3. Using the inverse FFT. When inverting the y-FT, we use the formula (2.2) and we can take advantage of the low computational complexity of the inverse fast Fourier transform (IFFT). Specifically, we use the MATLAB procedure `ifft`. The details of our implementation of `ifft` are described in the appendix of [13].

5.4. Numerical experiments. In this section, we perform numerical experiments to test the quadratic convergence in Δx and the exponential convergence in Δp, asserted in Theorem 3.1 and section 5.2, respectively.

By taking the double inverse Fourier transform (in s and p) of V in (3.4), one finds the exact solution to (1.4),

$$u(x,y,t)=\frac{\sqrt{3}}{2\pi t^2}\exp\left(-\frac{1}{4t}x^2\right)\exp\left(-\frac{3}{t^3}\left(y-\frac{t}{2}x\right)^2\right),\quad (x,y)\in\mathbb{R}^2,\ t>0,$$

with which the numerical solution can be compared (see also [9]).

In Figure 4, we monitor the convergence as $\Delta x\to 0$ for a range of values of Δp, which correspond to $n_p=36,40,44,48,52$. Here, we have chosen a finite x-range of $[-10,10]$ with n_x equally spaced mesh points, and the p-range as $[-20,20]$.

For large enough n_p, e.g., $n_p=52$, the plot shows quadratic convergence to the true solution. However, for a given value of Δp, quadratic convergence only continues to hold, as $\Delta x\to 0$, up to a critical value of Δx, beyond which the decay of the discretization error stops. Consequently, we need to reduce Δp appropriately in order

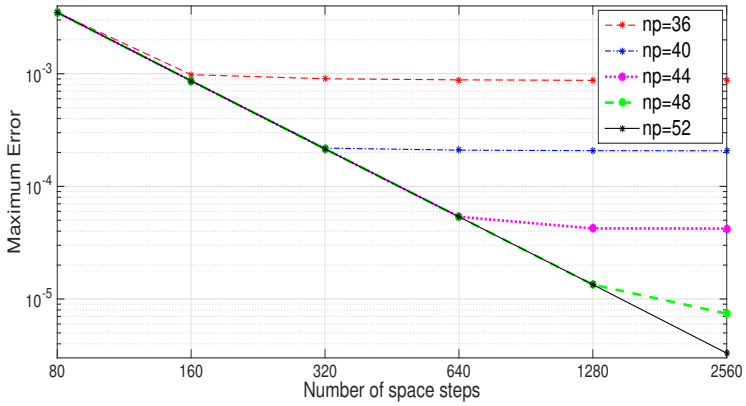

FIG. 4. *Toy model: maximum error in the semidiscrete Fourier method against the number of spatial steps. We show the effect of the choice of n_p on the accuracy of the y-FT and the resulting convergence in $\Delta x \to 0$.*

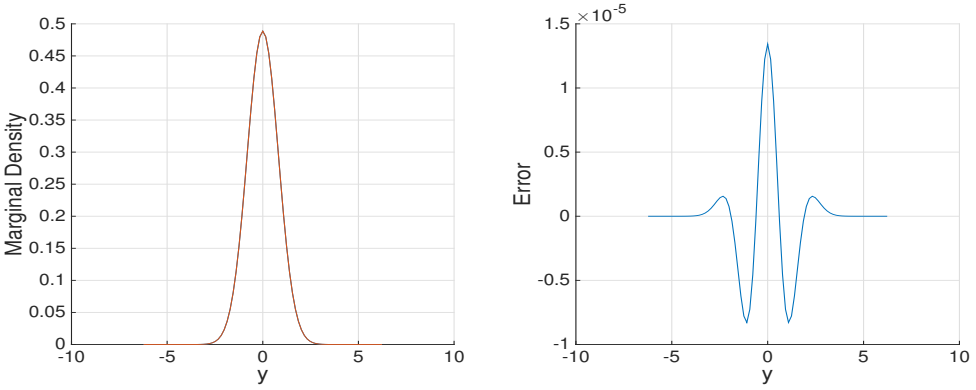

FIG. 5. *Toy model approximated by the semidiscrete Fourier method using the matrix exponential. Left, the marginal y-density for $x \in [-20, 20]$, $p \in [-20, 20]$, $n_x = 2560$, $n_p = 80$. Right, the difference between numerical and exact solutions.*

to achieve a satisfactory degree of accuracy. We deduced in section 5.2 the exponential convergence in Δp and a practical rule to choose n_p with an arbitrarily small power of n_x. Indeed, the horizontal asymptotes for large n_x are roughly equally spaced on a log-scale when n_p increases by a constant step, in line with the theoretical prediction.

In certain applications u is interpreted as a joint probability density of two variables and one is interested in the marginal density in y (see [13, section 5]). It also simplifies the visualization of the errors. The numerical solution, U, at time $T > 0$, is calculated at grid points (x_j, y_k) and is then numerically integrated over x to give the marginal probability distribution for y.

Figure 5, left, plots the true and numerical marginal densities, while Figure 5, right, shows the difference between the marginal densities of the true and numerical solutions. We took $x \in [-20, 20]$ and $p \in [-20, 20]$ with 80 grid points in the p-direction and 2560 grid points in the x-direction.

The marginal y-density is found to be Gaussian with mean 0 and variance $2t^3/3$, and, integrating (3.1) over $\mathbb{R}$ with respect to x, the numerical error is to leading-order proportional to its fourth y-derivative. This is precisely what is seen in Figure 5.

The computing times on a MacBook Pro 2.2 GHz with 1 processor and 4 cores, 16 Gbytes of RAM for 160, 320, 640, and 1280 mesh points and $n_p = 52$ were 2.9, 9.6, 60.1, and 356.5 seconds, respectively. The algorithm consists of the computation of a matrix exponential with dimension equal to the number of mesh points, independently for n_p different values of p, and an FFT with n_p points, which has log-linear complexity in n_p. Due to the fast convergence in n_p, for the mesh parameters considered here, the last step is negligible. From the times above, it appears that the complexity of computing the matrix exponential is roughly of order 2.5.

5.5. A fully discrete Fourier scheme. Just as its semidiscrete counterpart, the fully discrete Fourier scheme uses the y-FT to reduce the dimension of the problem, but it then applies discretization in both the x- and t-direction. After solving the linear system we again invert the y-FT to obtain our approximate solution, $U(x_j, y, t_l)$, for the original problem. Here $t_l = l\Delta t$ are equally spaced time steps. We use the toy model described above to study this scheme.

We discretize (2.3) in the x-direction, using equally spaced grid points, to obtain (2.5), and then in the t-direction, using the (semi)implicit Euler scheme, to obtain

$$\frac{V_j^{n+1}(p,t) - V_j^n(p,t)}{\Delta t} - ipx_j V_j^{n'}(p,t) = \frac{V_{j+1}^{n+1}(p,t) - 2V_j^{n+1}(p,t) + V_{j-1}^{n+1}(p,t)}{\Delta x^2},$$

subject to homogeneous Dirichlet boundary conditions at the endpoints of the x-range, where $n' = n$ if the drift term is treated explicitly and $n' = n+1$ if it is treated implicitly. In the former case, the finite difference scheme can be shown to be conditionally stable in the ℓ^2 norm provided that $\Delta t = \mathcal{O}(\Delta x^2)$ and $|p| = \mathcal{O}(\Delta x^{-r})$ with $r \in (0,1)$, while in the latter case it is unconditionally stable in the ℓ^2 norm. Obviously, other time discretizations are also possible, such as second- or higher-order backward differentiation formulae, but for the sake of simplicity of the discussion we shall focus here on time stepping via the Euler scheme.

Remark 5. For the purposes of an error analysis along the lines of section 3, we would apply the semidiscrete x-FT to obtain

$$\frac{W^{n+1}(s,p,t) - W^n(s,p,t)}{\Delta t} - p\frac{\partial W^{n'}(s,p,t)}{\partial s} = -W^{n+1}(s,p,t)\frac{4\sin^2\left(\frac{s\Delta x}{2}\right)}{\Delta x^2},$$

which can then be written as

$$f(s)\, W^{n+1}(s,p,t) - p\Delta t\frac{\partial W^{n'}(s,p,t)}{\partial s} = W^n(s,p,t),$$

where $f(s) = 1 + 4\lambda\sin^2\left(\frac{s\Delta x}{2}\right)$ and $\lambda = \frac{\Delta t}{\Delta x^2}$. This equation is a "differential recursion" for the double-FT in the explicit case ($n' = n$) and an "integral recursion" in the implicit case ($n' = n+1$). Although it is possible to identify leading-order terms heuristically by an expansion, the rigorous convergence analysis of these fully discrete schemes in the presence of a Dirac initial datum has proved elusive due to the complexity of the error propagation over the time steps across wavenumbers. We shall therefore explore these schemes by way of numerical tests.

We present the results obtained by applying the two methods above to the model PDE under consideration. As with the semidiscrete Fourier method, the solution for U is first integrated over x, before being plotted against y. We took $x \in [-20, 20]$, $p \in [-20, 20]$, $t \in [0, 1]$ with $n_x = 1800$ grid points in the x-direction, $n_p = 80$ grid points in the p-direction, and $n_t = 10240$ grid points in the t-direction.

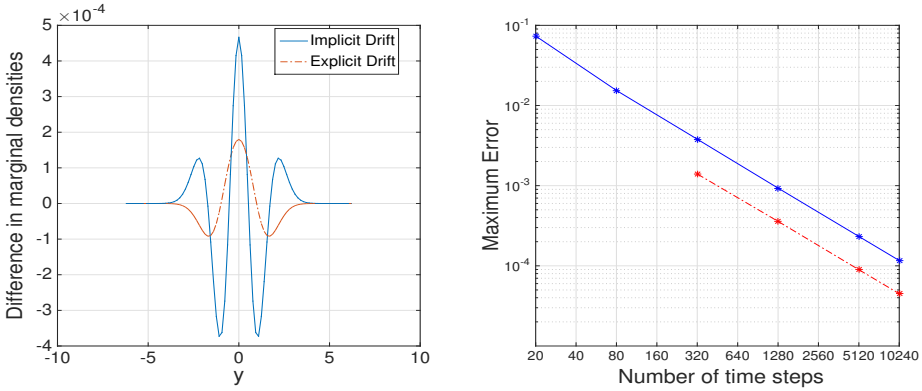

FIG. 6. *Toy model approximated by the discrete Fourier method with an explicit and implicit approximation for the drift term. Left, the difference between the exact and approximate solutions with* $x \in [-20, 20]$, $p \in [-20, 20]$, $t \in [0, 1]$, $n_x = 1800$, $n_p = 80$, $n_t = 10240$. *Right, with the other parameters taken to be the same, the error for decreasing time step* Δt *with* $\Delta t/\Delta x^2$ *held constant.*

The left plot of Figure 6 shows the difference between the true and numerical solutions. In the absence of an asymptotic result on the leading-order error term (as we had in the semidiscrete case) it is harder to interpret the spatial shape of these errors. The truncation error of the implicit Euler scheme is given by $-\Delta t\ \frac{1}{2}u_{tt}$, while for the explicit treatment of the drift term (but implicit diffusion term), the truncation error is $\Delta t\ \left(\frac{1}{2}u_{tt} - \frac{1}{2}x\,u_{ty}\right)$. The numerical results suggest that the combination of these two terms, together with the spatial error, leads to a smaller maximum error of the explicit scheme. The functional form of the leading error seen in Figure 6, which can be derived in principle by convolution of the truncation error, known explicitly from the closed-form solution, with the fundamental solution of the PDE, and integration over the x-variable, is not very insightful.

Finally, the right plot of Figure 6 shows the convergence rate for the solutions as the grid is refined with $\lambda = \frac{\Delta t}{\Delta x^2}$ held constant. Due to the stiffness of the ODE system (5.1) for large p and for large L, there is an upper bound on the time step, depending on the range of p and x, which has to be satisfied on order to obtain meaningful solutions with the explicit treatment of the drift, and this is irrespective of the fact that we are already keeping $\Delta t/\Delta x^2$ constant in our refinement. We observe asymptotic first-order convergence in time for both schemes, where the error is evaluated in the maximum norm. The slope of the last two points of the log-log plot is 1.00 in both cases.

The computing times for the explicit treatment of the drift for 640, 905, 1280, and 1800 space steps and $n_p = 80$ were 10.2, 24.5, 62.3, and 170.0 seconds, respectively, and almost identical for the implicit treatment. Given the choice of the time steps in relation to the space steps, the time increases by roughly a factor of eight if the number of space steps is doubled, resulting in a cubic complexity. This is asymptotically slightly worse than the semidiscrete method, but the absolute times were significantly lower for parameters in the practical range.

6. Conclusions. The numerical analysis of hypoelliptic PDEs with variable coefficients and Dirac initial datum is notoriously difficult because standard approaches to convergence analysis are not directly applicable. In contrast with parabolic initial-value problems, in the case of hypoelliptic PDEs the situation is complicated by the fact that diffusion generally acts only in some, but not all, co-ordinate directions.

The approach of [3] for the one-dimensional heat equation with Dirac datum is based on Fourier analysis to show approximation of a certain order for the low wavenumber components and exponential decay of the high wavenumber components for smoothing schemes. In the present case of hypoelliptic equations the analysis is more intricate because of the interplay of wavenumbers in the different co-ordinate directions as a consequence of variable coefficients and the resulting noncommutativity of the spatial differential operators in the different directions.

We exploit the special structure of the Kolmogorov equations under consideration by performing a Fourier transform in the direction with the pure transport term and discretize in the diffusive direction(s) by a finite difference scheme. This results in a parametrized system of semidiscrete equations, which can be solved by standard methods, and the resulting solution is then transformed back from Fourier space using exponentially convergent numerical quadrature, thus leading to an effective technique for dimensional reduction. The numerical analysis sheds light on the interaction of different wavenumbers and allows us to derive second-order convergence for the proposed numerical scheme in the absence of time-discretization.

An open question at present is how to replicate the analysis herein for the fully discrete counterpart of the method, which also includes time-discretization. Although unconditional stability in the ℓ^2 norm of the implicit Euler scheme and conditional stability, with $\Delta t = \mathcal{O}(\Delta x^2)$ and $|p| = \mathcal{O}(\Delta x^{-r})$ with $r \in (0,1)$, of the explicit Euler scheme can be proved by standard energy estimates (cf. [8, section 3.2.2]), a similar argument does not seem to apply in the case of Dirac initial datum, as the use of a discrete negative-order Sobolev norm, which would be the natural choice of norm for the discrete representation of the Dirac function on the finite difference grid, in conjunction with discrete counterparts of parabolic smoothing estimates in the diffusive directions, is obstructed by the particular form of the variable coefficients in the Kolmogorov equations under consideration, and the complex nature of error propagation for the fully discrete scheme has not so far allowed a rigorous convergence analysis of the fully discrete scheme.

Acknowledgment. The second author thanks the Nečas Center at the Charles University in Prague for the stimulating research environment during his sabbatical leave.

REFERENCES

[1] A. Bermúdez, M. R. Nogueiras, and C. Vázquez, *Numerical analysis of convection-diffusion-reaction problems with higher order characteristics finite elements. Part* I*: Time discretization*, SIAM J. Numer. Anal., 5 (2006), pp. 1829–1853.

[2] O. Bokanowski and G. Simarmata, *Semi-Lagrangian discontinuous Galerkin schemes for some first- and second-order partial differential equations*, ESAIM Math. Model Numer Anal., 50 (2016), pp. 1699–1730.

[3] R. Carter and M. B. Giles, *Sharp error estimates for discretizations of the* 1*D convection-diffusion equation with Dirac initial data*, IMA J. Numer. Anal., 27 (2007), pp. 406–425.

[4] E. L. Foster, J. Lohéac, and M.-B. Tran, *A structure preserving scheme for the Kolmogorov–Fokker–Planck equation*, J. Comput. Phys., 330 (2017), pp. 319–339.

[5] M. B. Giles, *Sharp Error Estimates for a Discretisation of the* 1*D Convection-Diffusion Equation with Dirac Initial Data*, Technical report 04-17, Oxford University Computing Laboratory, 2004, https://people.maths.ox.ac.uk/gilesm/files/NA-04-17.pdf.

[6] N. J. Higham, *The scaling and squaring method for the matrix exponential revisited*, SIAM J. Matrix Anal. Appl., 26 (2005), pp. 1179–1193.

[7] L. Hörmander, *Hypoelliptic second order differential equations*, Acta Math., 119 (1967), pp. 147–171.

[8] B. S. Jovanović and E. Süli, *Analysis of finite difference schemes for linear partial differential equations with generalized solutions*, Springer Ser. Comput. Math. 46, Springer, New York, 2014.

[9] A. Kolmogorov, *Zufällige Bewegungen (Zur Theorie der Brownschen Bewegung)*, Ann. of Math., 35 (1934), pp. 116–117.
[10] S. Larsson and V. Thomée, *Partial Differential Equations with Numerical Methods*, Vol. 45, Springer, New York, 2008.
[11] F. W. J. Olver, *NIST Handbook of Mathematical Functions*, Cambridge University Press, Cambridge, 2010.
[12] A. Porretta and E. Zuazua, *Numerical hypocoercivity for the Kolmogorov equation*, Math. Comp., 86 (2017), pp. 97–119.
[13] C. Reisinger, E. Süli, and A. Whitley, *A Partial Fourier Transform Method for a Class of Hypoelliptic Kolmogorov Equations*, preprint, arXiv:1604.05268, 2016.
[14] C. Reisinger and A. Whitley, *The impact of a natural time change on the convergence of the Crank–Nicolson scheme*, IMA J. Numer. Anal., 34 (2014), pp. 1156–1192.
[15] E. Süli and D. F. Mayers, *An Introduction to Numerical Analysis*, Cambridge Univerity Press, Cambridge, 2006.
[16] E. Süli and A. F. Ware, *A spectral method of characteristics for hyperbolic problems*, SIAM J. Numer. Anal., 28 (1991), pp. 423–445.
[17] L. N. Trefethen and J. A. C. Weideman, *The exponentially convergent trapezoidal rule*, SIAM Rev., 56 (2014), pp. 385–458.
[18] C. Villani, *Hypocoercive diffusion operators*,, in Proceedings of the International Congress of Mathematicians 3, 2006, pp. 473–498.
[19] C. Villani, *Hypocoercivity*, Mem. Amer. Math. Soc. 950, AMS, Providence, RI, 2009.